Nanoclusters

Deutsche Ausgabe: DOI: 10.1002/ange.202001034
Internationale Ausgabe: DOI: 10.1002/anie.202001034

Giant Emission Enhancement of Solid-State Gold Nanoclusters by Surface Engineering

Chuanhao Yao[+], Cong-Qiao Xu[+], In-Hyeok Park, Meng Zhao, Ziyu Zhu, Jing Li, Xiao Hai, Hanyan Fang, Yong Zhang, Gennevieve Macam, Jinghua Teng, Lin Li, Qing-Hua Xu, Feng-Chuan Chuang, Junpeng Lu, Chenliang Su, Jun Li* und Jiong Lu**

Abstract: *Ligand-induced surface restructuring with heteroatomic doping is used to precisely modify the surface of a prototypical $[Au_{25}(SR^1)_{18}]^-$ cluster (**1**) while maintaining its icosahedral Au_{13} core for the synthesis of a new bimetallic $[Au_{19}Cd_3(SR^2)_{18}]^-$ cluster (**2**). Single-crystal X-ray diffraction studies reveal that six bidentate $Au_2(SR^1)_3$ motifs (L2) attached to the Au_{13} core of **1** were replaced by three quadridentate $Au_2Cd(SR^2)_6$ motifs (L4) to create a bimetallic cluster **2**. Experimental and theoretical results demonstrate a stronger electronic interaction between the surface motifs ($Au_2Cd(SR^2)_6$) and the Au_{13} core, attributed to a more compact cluster structure and a larger energy gap of **2** compared to that of **1**. These factors dramatically enhance the photoluminescence quantum efficiency and lifetime of crystal of the cluster **2**. This work provides a new route for the design of a wide range of bimetallic/alloy metal nanoclusters with superior optoelectronic properties and functionality.*

Introduction

Luminescent metal nanoclusters consisting of an atomically precise metal core and ligand shell show size- and composition-dependent optical and electronic properties with a great potential to be used in optoelectronic and biomedical applications.[1] However, the luminescence quantum yields (QY) of metal nanoclusters are generally low.[2] Numerous efforts have been devoted to develop various strategies for the improvement of the light-emitting properties of metal nanoclusters over the last two decades.[3] For instance, Wu et al. reported that the ligands play a pivotal role in enhancing the PL of $Au_{25}(SR)_{18}$ nanocluster attributed to the ligand-to-metal charge transfer (LMCT).[2a] Pramanik et al. demonstrated that metal-to-ligand charge transfer (MLCT) also can be used to greatly increase the luminescence QY of gold nanoclusters.[3a] Apart from ligand engineering, doping of metal nanoclusters with heteroatom(s) offers a new approach for PL enhancement. For example, a substitution of gold with silver atoms for the Au_{25} nanocluster can drastically enhance the intensity of its photoluminescence.[3b] Apart from this, aggregation-induced emission (AIE) arising from the restriction of intramolecular rotation has emerged as a highly promising strategy to improve the PL of metal nanoclusters. For example, Xie et al. reported a facile one-pot synthesis of highly luminescent Au-thiolate nanocluster with a high QY of about 15% attributed to the AIE.[3c,d] Pyo et al. also reported a gold nanocluster derived from $Au_{22}(SG)_{18}$ cluster with a QY greater than 60%, by rigidifying its gold shell with tetraoctylammonium (TOA) cations.[3e] Gan et al. also demonstrated that $Au_{24}(SR)_{20}$ with rigid ligands shows a dramatically enhanced PL.[3f] The aforementioned strategies, including ligand

[*] Dr. C. Yao,[+] Dr. C. Su
SZU-NUS Collaborative Center and International Collaborative Laboratory of 2D Materials for Optoelectronic Science & Technology of Ministry of Education, Engineering Technology Research Center for 2D Materials Information Functional Devices and Systems of Guangdong Province, Institute of Microscale Optoelectronics Shenzhen University, Shenzhen 518060 (China)
E-Mail: chmsuc@szu.edu.cn
Dr. C. Yao,[+] Dr. L. Li
Shaanxi Key Laboratory of Flexible Electronics (KLoFE), Institute of Flexible Electronics, Northwestern Polytechnical University Xi'an 710072 (China)
Dr. C. Yao,[+] Dr. I.-H. Park, Z. Zhu, Dr. J. Li, Dr. X. Hai, H. Fang, Dr. Q.-H. Xu, Dr. J. Lu
Department of Chemistry, National University of Singapore 3 Science Drive 3, Singapore 117543 (Singapore)
E-Mail: chmluj@nus.edu.sg
Dr. C.-Q. Xu,[+] Prof. J. Li
Department of Chemistry
Southern University of Science and Technology
Shenzhen 518055 (China)
Prof. J. Li
Department of Chemistry, Tsinghua University
Beijing 100084 (China)
E-Mail: junli@tsinghua.edu.cn
Dr. M. Zhao, Dr. J. Teng
Institute of Materials Research and Engineering (IMRE)
Agency for Science, Technology and Research (A*STAR)
Singapore 138634 (Singapore)
Y. Zhang, Dr. J. P. Lu
School of Physics, Southeast University
Nanjing 211189 (China)
G. Macam, Prof. F.-C. Chuang
Department of Physics, National Sun Yat-Sen University
Kaohsiung 80424 (Taiwan)
[+] These authors contributed equally to this work.
Supporting information and the ORCID identification number(s) for the author(s) of this article can be found under: https://doi.org/10.1002/anie.202001034.

engineering, heteroatom doping, and rigidification of ligand shell and AIE mainly rely on the strong intramolecular interactions. In contrast, non-covalent weak intermolecular interactions, such as hydrogen bonding and C–H···π interaction, also play important roles in regulating the light-emitting properties of metal nanoclusters. Chen et al. reported that the noble metal nanocluster (Au_4Ag_{13}) exhibits a crystallization induced emission enhancement arising from non-covalent C–H···π interactions. These weak interactions restrict the intramolecular rotations and vibrations, which thus prompt the radiative transitions in the crystalline state.[3g]

Herein, we develop a new surface-engineering approach involving a combination of the strategies discussed above towards a dramatic emission enhancement of a new bimetallic nanocluster. We chose $Au_{25}(SR)_{18}$ (a well-studied nanocluster[4]) as precursor to prepare this bimetallic cluster with enhanced light-emitting properties by ligand engineering combined with heteroatom doping. Cd was used as a heteroatom dopant, together with a bulky ligand, *p*-toluenethiol, for the ligand exchange with original one (2-phenylethanethiol). A core–shell structured $Au_{25}(SR^1)_{18}$ (**1**) cluster (SR^1 = 2-phenylethanethiol)[4] can be readily converted into a new bimetallic $Au_{19}Cd_3(SR^2)_{18}$ (**2**) cluster (SR^2 = *p*-toluenethiol) via the surface engineering that involves the doping with Cd in combination with the ligand induced surface reconstruction. In this process, the surface motifs ($Au_2(SR^1)_3$) attached to a metal core (Au_{13}) are replaced by $Au_2Cd(SR^2)_6$, while the structural integrity of metal Au_{13} core are maintained. Here, this new motif ($Au_2Cd(SR^2)_6$) contain Au^I and Cd^{II} species. The Au_{13} core as a superatom[5] shows a much stronger electronic mixing with new motifs $Au_2Cd(SR^2)_6$, compared to $Au_2(SR^1)_3$, resulting in a wider energy gap with dramatically enhanced stability and light emission of the bimetallic cluster **2**. Both experimental data and quantum-chemical calculations reveal that **2** undergoes a significant structural contraction upon surface engineering as compared to that of the precursor **1**. This further suggests the existence of a stronger core–shell electronic interaction in **2**, which accounts for the emission enhancement.

Results and Discussion

A typical synthesis process of **2** involves two critical steps: 1) crystals of **1** were first dissolved in toluene and then mixed with an aqueous solution of cadmium acetate; 2) subsequently, excess *p*-toluenethiol was added in the above solution. The reaction was aged for 1 hour at 60 °C (see the Supporting Information for more details). To better understand the cluster conversion process, we performed time-dependent UV/Vis/NIR spectroscopic measurement of reaction mixtures. The reaction occurs very rapidly as evidenced by the disappearance of the characteristic adsorption features of the precursor **1** (Supporting Information, Figure S1). The emergence of completely new absorption features in UV/Vis/NIR spectrum suggests a successful synthesis of a new cluster with distinct electronic and optical properties.

To determine its precise structure, we attempted the crystallization of the as-synthesized cluster using a typical recipe

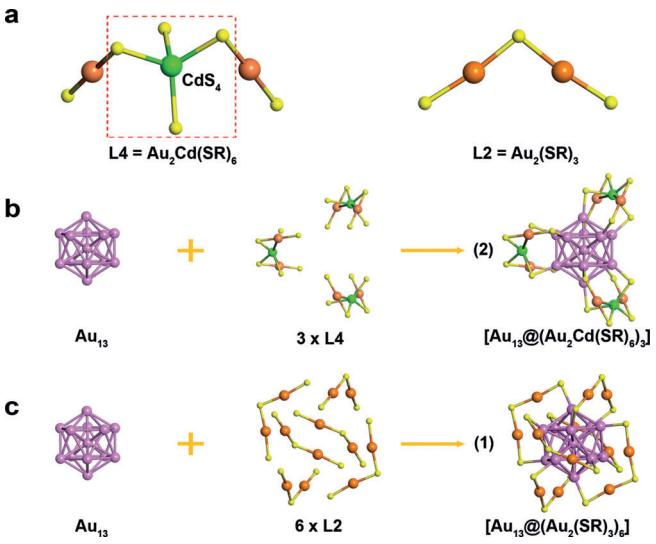

Figure 1. Structure analysis of clusters **1** and **2**. a) Surface motifs of $Au_2Cd(SR)_6$ (left) and $Au_2(SR)_3$ (right); b) structure analysis of **2**; c) structural anatomy of **1**. Au magenta/gold, Cd green, S yellow; C and H atoms and the counter ion, $[N(C_8H_{17})_4]^+$, are omitted for clarity.

involving the diffusion of methanol into a toluene-based cluster solution. Red block crystals were obtained after two weeks with a yield of about 90% (Supporting Information, Figure S2). Single-crystal X-ray diffraction (SXRD) analysis reveals that the unit cell of the crystal contains two enantiomer of **2** (Supporting Information, Figure S3) packed under a space group of *P*2/*c* (see the Supporting Information) and **2** consists of three $Au_2Cd(SR)_6$ motifs (L4; Figure 1 a) attached to an Au_{13} icosahedron core (Figure 1 b) in a quadridentate coordination configuration, whereas six bidentate $Au_2(SR)_3$ motifs staple on the Au_{13} core of **1** (Figure 1 c). For **2**, each surface motif ($Au_2Cd(SR)_6$) is composed of a blende structured $Cd(SR)_4$ subunit (Figure 1 a) which has not been observed in other AuCd bimetallic clusters before.[6] We note that both the precursor **1** and **2** contain a nearly identical Au_{13} core, which suggests the mother cluster is transformed into a new cluster by surface engineering (Figure 1 b,c). We also found that a positively charged counter ion, $[N(C_8H_{17})_4]^+$, is associated with each cluster in the single crystal (Supporting Information, Figure S4). This indicates that cluster **2** bears one negative charge, as evidenced by the electrospray ionization mass spectrometry (ESI-MS) analysis (Supporting Information, Figure S5). Such a negative charge state is consistent with the Au^I and Cd^{II} valence state in the L4 ligand, thus rendering a closed-shell electronic configuration[4d,7] of Au_{13}^{5+} ($8e^-$) for **2** with a high chemical stability, as will be further discussed below.

We then investigated the electronic and optical properties of **2** in comparison with that of the precursor **1**. It is found that optical adsorption spectrum of **2** is distinct from that of **1** (Figure 2). The absorption peaks of **1** are observed at 3.08 eV, 2.74 eV, 1.79 eV with a shoulder peak at 1.59 eV (Figure 2 a). Extrapolation of the absorption spectrum to zero absorbance yields a HOMO–LUMO gap of about 1.35 eV, in good agreement with a previous report.[8] The UV/Vis spectrum of **2** exhibits three absorption features peaked around

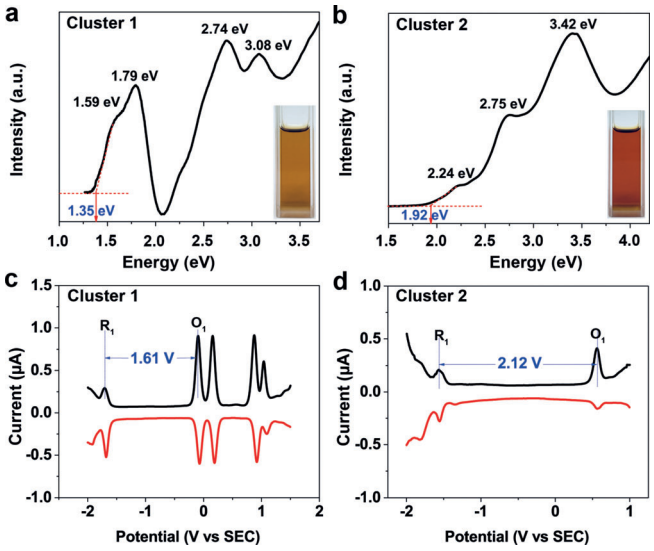

Figure 2. Optical properties and differential pulse voltammetry (DPV) analysis of clusters **1** and **2**. a),b) UV/Vis/NIR spectra of a) **1** and b) **2** clusters. Insets: photographs of the **1** and **2** clusters dissolved in dichloromethane. c),d) DPV of c) **1** and d) **2**.

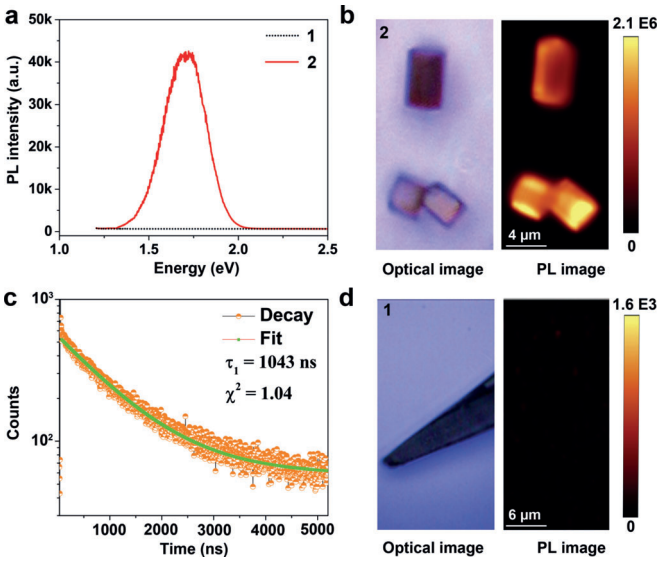

Figure 3. Probing the light emitting properties of the crystals of **2**. a) Photoluminescence (PL) emission spectra of **1** and **2** crystals; b) PL image of **2**; c) PL decay curve of **2**. The PL image of the crystals of **1** is shown in (d) for comparison.

3.42 eV, 2.75 eV, and 2.24 eV. The HOMO–LUMO gap of **2** is determined to be 1.92 eV based on its optical adsorption edge (Figure 2b). The electrochemical gaps of these two clusters are evaluated using differential pulse voltammetry (DPV).[8] The energy difference between the first oxidation (O_1) peak and the first reduction (R_1) peak yields the electrochemical gap of the cluster. As shown in Figure 2c, the electrochemical gap of **1** is measured to be 1.61 V, consistent with a previous report.[8] In contrast, the electrochemical gap of **2** is enlarged to 2.12 V (Figure 2d). Hence, both optical adsorption and DPV measurement reveal that **2** exhibits a larger energy gap upon surface engineering as compared to that of the mother cluster **1**.

The oxidation of **2** occurs at a more positive potential (0.56 V) compared to that of **1** (−0.1 V), indicating a higher oxidation barrier for **2** (Figure 2c,d). We further probed the stability of these two clusters against the chemical oxidation using a typical oxidation agent, *tert*-butyl hydroperoxide (TBHP). Upon adding TBHP in the solution, a dramatic change of the absorption spectrum of **1** occurs in a few minutes, attributed to a rapid chemical oxidation and decomposition of **1**. In contrast, the optical absorption spectra of **2** remain nearly constant for more than 48 h, validating a superior stability of the cluster **2** (Supporting Information, Figure S6).

As mentioned above, the bimetallic cluster **2** can be viewed as a core–shell structured gold cluster integrated with CdS_4 subunits on the surface. Such a unique structure motivates us to probe its light emission properties. As shown in the Supporting Information, Figure S7, cluster **2** dispersed in dichloromethane shows an emission peak at about 1.6 eV, while **1** dispersed in the same solvent exhibits a broader peak ranging from 1.53 to 1.66 eV. The PL quantum yields (QY) of **2** in the solution phase is about 10-fold higher than that of **1**. More interestingly, the single crystal of **2** shows a dramatically enhanced emission as shown in Figure 3a. The PL quantum yield of the single crystal of **2** is determined to be 9.8%, whereas the PL quantum yield of the single crystal of **1** is extremely low, being virtually below the detection limit. Furthermore, the spatial PL map of the crystals of **2** (excited by a 532 nm laser) also reveals a strong emission over the whole crystal (Figure 3b). In contrast, PL map of the crystal of **1** appears dark and featureless at the similar conditions, due to an extremely low PL quantum efficiency (Figure 3d). All of these observations suggest a remarkable crystallization-induced emission enhancement (CIEE)[3g,10] for cluster **2**. Furthermore, temperature-dependent PL measurement reveals that the emission peak of **2** is measured to be 1.64 eV at 77 K and gradually increases to 1.72 eV at 297 K (Figure 4a). Such a temperature-dependent blue-shift in the emission of the single crystal of **2** is distinct from the majority of metal clusters reported such as Au_{25} and Au_{38}.[11]

To gain a better understanding of the electronic and optical properties of **2**, we performed quantum chemical calculations using density functional theory (DFT) to study its energy-level correlation diagram of Kohn–Sham molecular orbitals (MO) between Au_{13} icosahedron and the $[Au_2Cd(SR)_6]_3$ shell (note: R = H is used to reduce the computational cost). As shown in Figure 5b and the Supporting Information, Figure S8, the HOMO and LUMO orbitals of $Au_{13}@[Au_2Cd(SH)_6]_3^-$ are mainly derived from 5d atomic orbitals (AOs) and of 6s AOs of Au atoms in the Au_{13} icosahedron, respectively. The calculation yields a HOMO–LUMO gap of 2.06 eV (Figure 5b), in a reasonably good agreement with the energy gap (1.92 eV) determined from optical absorption spectrum. As can be seen from the energy-level correlation diagram shown in the Supporting Information, Figure S9, the Au_{13} core of $Au_{13}@[Au_2Cd(SH)_6]_3^-$ cluster has a pseudo-icosahedral structure. The superatom Au_{13}^{5+} unit will be extremely stable, with a $1S^21P^61D^0$ configuration for atomic 6s

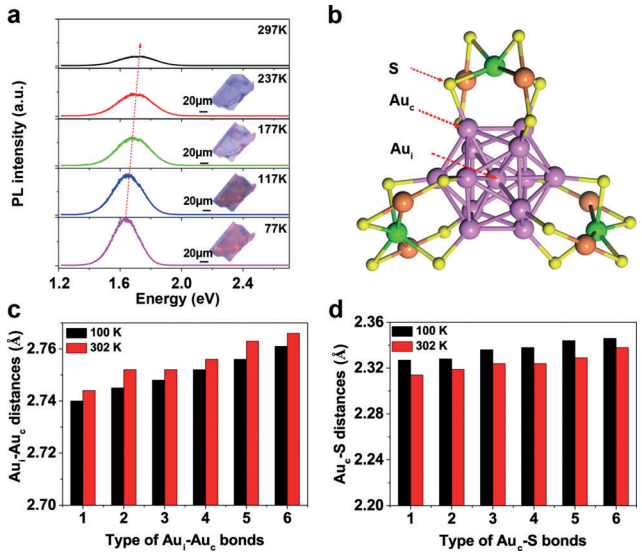

Figure 4. a) Temperature-dependent emissions of the crystal of **2**. b) Structure of $Au_{19}Cd_3S_{18}$ framework in cluster **2**, where the center (Au_i), vertices (Au_c), and S atoms are indicated. c) Au_i–Au_c distances of Au_{13} core at 100 K and 302 K, respectively. d) Au_c–S distances at 100 K and 302 K, respectively.

group orbitals in the spherical jellium model.[12] A direct comparison of calculated MO energy-level diagrams of the model clusters $Au_{13}@[Au_2(SH)_3]_6^-$ and $Au_{13}@[Au_2Cd(SH)_6]_3^-$ provides interesting insights into their different HOMO–LUMO gap sizes. Like the orbital distributions of **1**, the D orbitals of **2** split into five degenerate orbitals (LUMO, LUMO + 1, LUMO + 2) considering the ligand field effect,[1d,4c,13] as shown in Figure 5 a,b and the Supporting Information, Figure S8. Compared with Au_{13}^{5+} of D_3-$Au_{13}@[Au_2Cd(SH)_6]_3^-$, the HOMO–LUMO gap of Au_{13}^{5+} of *Ci*-$Au_{13}@[Au_2(SH)_3]_6^-$ is slightly smaller due to its expanded size of the icosahedron core and the decreased symmetry. Smaller ligand-field splitting of the LUMOs of Au_{13}^{5+} will contribute to a larger HOMO–LUMO gap of $Au_{13}@[Au_2Cd(SH)_6]_3^-$. Furthermore, the LUMO of $Au_{13}@[Au_2(SH)_3]_6^-$ is destabilized by interactions between the LUMO of Au_{13}^{5+} and a low-lying filled orbital of the $Au_2(SR)_3$ shell (Figure 5 a). Owing to a large energy separation of these two weakly interacting orbitals, the LUMO of cluster **1** is not destabilized as much as in **2**, which reduces the HOMO–LUMO gap of cluster **1** to 1.26 eV. Comparably, a smaller separation of two interesting orbitals including LUMO of the Au_{13} core and high-lying $Au_2Cd(SH)_6$ orbital leads to a stronger shell-metal core interaction in $Au_{13}@[Au_2Cd(SH)_6]_3^-$, which gives rise to the increased HOMO–LUMO gap and stability.

The last question remaining to be addressed is the physical origin of the dramatically enhanced PL of cluster **2**. Such an effect can be ascribed to its unique core–shell structure with a strong core–shell electronic mixing. Au_{13} kernel of **2** is contracted compared to that of **1** as revealed by SXRD data (Supporting Information, Figure S10). The averaged Au–Au distance between center (Au_i) and vertices (Au_c) Au atoms of icosahedron in **2** is 2.750 Å, shorter than that of **1** (2.775 Å; Supporting Information, Figure S10c); Furthermore, the Au–S bond between the vertices Au atoms (Au_c) of Au_{13} core and S atom of ligand are shortened from 2.37 Å (for **1**) to 2.34 Å for **2** (Supporting Information, Figure S10d), indicating stronger binding. Very recently, Liu et al. also found that a change of Au–S bond length can dramatically affect the luminescence of the complexes. A decrease of the Au–S bond length was associated with an increase of the luminescence intensity,[14] similar to our observations. Apart from the change of Au–S bond length, the size of Au_{13} core (Au_i–Au_c distances) also plays an important role in the emission enhancement observed here. A more compact core–shell

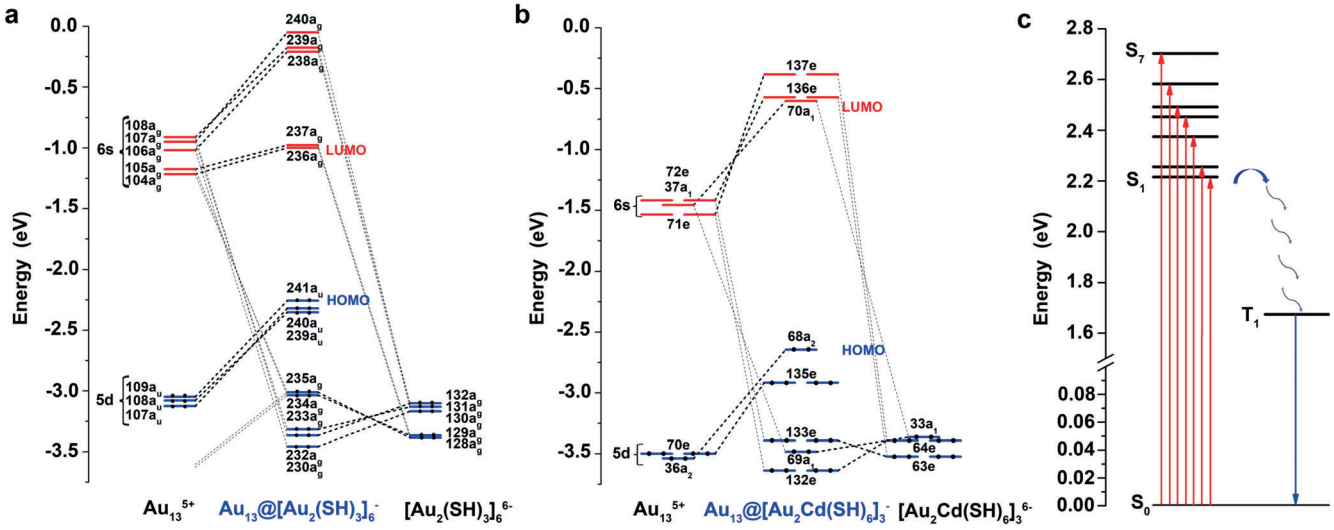

Figure 5. a) Kohn–Sham molecular orbital (MO) energy-level correlation diagram of $Au_{13}@[Au_2(SH)_3]_6^-$ and b) $Au_{13}@[Au_2Cd(SH)_6]_3^-$. Blue and red lines represent occupied and empty orbitals, respectively. Wide and thin dashed lines represent the primary and secondary contributions. Electrons on the occupied MOs are marked as dots. c) Electron excitations of $Au_{13}@[Au_2Cd(SH)_6]_3^-$, with the excitation energies obtained from TDDFT calculations. S_0 represents the ground state and S_n (n = 1–7) shows the excited singlet state. Red arrows indicate the excitations from S_0 to S_n and blue arrows indicate the phosphorescence emission from the first excited triplet state (T_1).

structure of **2** can be attributed to the enhanced shell–metal core interaction and boosted PL intensity. We also compare the detailed structure of **2** at 100 K and 302 K. The results show that the Au_{13} core became even smaller at low temperature (Figure 4b,c), whereby the higher PL intensity can be obtained. However, the distances between Au_{13} core to shell (Au_c–S bond length) at 100 K are larger than that at higher temperature (Figure 4d). This indicates that the core–shell interaction of **2** is weakened as the temperature decreases, leading to the reduction of the energy gap, attributed to the red-shift of PL emission as the temperature decrease observed experimentally.

A dramatic PL enhancement of single crystal of cluster **2** can be associated with the rigidity of ligands and the unique packing of clusters in the crystal. First, individual cluster **2** adopts a propeller shape configuration with a relatively rigid ligand (*p*-toluenethiol), which reduces non-radiative decay of photoexcited electrons via restricting the vibration-assisted relaxation channels.[3g] Second, the distances of adjacent cluster–cluster separation in crystal of **2** is 15.500, 17.197, and 17.907 Å, which is shorter than that of **1** (16.156, 17.388, and 18.641 Å, respectively), resulting in a denser cluster packing in the crystal of **2** (Supporting Information, Figure S11). Furthermore, the clusters are further locked by intra-cluster C–H···π as well as inter-cluster π···π interactions (Supporting Information, Figure S12) in the crystalline state. Hence, the compact packing combined with the presence of ligand–ligand interactions effectively increases the energy barrier required to excite the vibration/rotations of ligands, whereby the PL quantum efficiency can be increased by suppressing the non-radiative channels. Moreover, crystals of **2** show a remarkably increased mono-exponential PL lifetime up to about 1.04 μs (Figure 3c). In contrast, the crystal of **1** shows a biexponential PL decay dynamics (0.8 ns and 2.3 ns).[9] This suggests that the electron relaxation pathway from excited state to ground state of **2** is different from that of **1**. To elucidate the micro-second lifetime of **2**, we performed time-dependent DFT (TDDFT) calculations to simulate the electron excitations from the ground state (S_0) and the emission peak position (Figure 5c; Supporting Information, Table S1). We can see that the lowest excitation energy from S_0 to the first excited singlet state (S_1) is about 2.22 eV. According to the excitation energy, the PL measured by a 532 nm (2.33 eV) laser can afford to the transitions including $S_0 \rightarrow S_1$, $S_0 \rightarrow S_2$, and $S_0 \rightarrow S_3$ excitation, despite the approximation of TDDFT method. These transitions involve the electronic excitations from the 5d (Au) dominated MOs to the 6s (Au) dominated MOs of the Au_{13} core, while the excitations to the ligand dominated MOs ($S_0 \rightarrow S_7$) require much higher energy photons. Single-point TDDFT emission energy calculations including spin–orbit coupling (SOC) for **2** at the optimized S_1 and T_1 geometries were performed, as shown in the Supporting Information, Table S2. Since the optimized S_1 and T_1 geometries are similar, the excitation energies and oscillator strengths are close. SOC-state 4 can be assigned to the S_1 state while SOC-states 1–3 are mainly derived from T_1 state. SOC-states 5–10 correspond to the components of the T_2 state. The excited state energies of S_1 and T_1 states are all lower than the experimental emission energy of 1.65 eV but within the error margin considering the typical underestimation of DFT excitation energy.[4c,15] Meanwhile, the calculated radiative lifetimes for T_1 states are about 300 times longer than for S_1 state, although the values are all larger than the experimental data due to approximation and simplification in the calculations. The calculated long lifetime of T_1 state further confirms the phosphorescence emission. Spin-flip TDDFT calculations of the first excited triplet state (T_1) show that the emission from T_1 to S_0 state will release about 1.67 eV, in good agreement with the experimental value (1.65 eV). It is also noted that the contribution of Cd atomic orbitals (AOs) to the LUMO and LUMO + 1 of T_1 state is non-negligible, presumably attributed to the long PL lifetime observed. To further prove this, we also carried out additional experiment to measure the PL emission of $Au_{19}Cd_3$ cluster single crystals in vacuum and in air. The results show that the emission intensity acquired in vacuum is much higher than that in air. This indicates a higher O_2 concentration tends to quench the PL emission of solid-state clusters. The new results further confirm a triplet emission of single crystal $Au_{19}Cd_3$ cluster (Supporting Information, Figure S13). Therefore, the surface engineering of **1** via Cd doping not only significantly boosts the PL quantum efficiency of **2** but also dramatically increases its PL lifetime due to the contribution of Cd 4d orbitals in the emission states.

Conclusion

We have demonstrated a new strategy for the surface engineering of metal clusters to tune their electronic and optical properties with atomic precision. Our approach involving the metal doping and ligand-induced structure reconstruction allows for the precise surface engineering of the metal cluster while keeping its superatom core unchanged for the synthesis of a bimetallic cluster with desired electronic and optical properties. By a judicious choice of both heteroatom dopant and rigid organic ligand, we have managed to replace the surface of a Au_{25} cluster of $[Au_{13}@(Au_2(SR^1)_3)_6]^-$ (**1**) with a unique surface motif consisting of blende structured CdS_4 subunit, whereby the chemical stability and light emission properties can be dramatically enhanced in the resulting $Au_{19}Cd_3$ core–shell cluster of $[Au_{13}@(Au_2Cd(SR^2)_6)_3]^-$ (**2**). Such a surface reconstructing not only results in a stronger orbital interaction between surface and metal core but also a denser packing of individual clusters in the single crystal, leading to a novel crystallization-induced emission enhancement (CIEE). Our findings may open up a new avenue for the surface engineering of metal clusters with precisely tunable chemical and physical properties.

Acknowledgements

J. Lu acknowledges the support from MOE grants (MOE2016-T2-2-020, MOE2017-T2-1-056 and R-143-000-A75-114) and NUS flagship green energy program. C.Y. acknowledges financial support from National Natural Science Foundation of China (21601193, 21703134), the Fundamental Research Funds for the Central Universities

(31020190QD013) and Postdoctoral Research Foundation of China (2017M612713). J.L. thanks the support from the National Natural Science Foundation of China (21590792, 91645203, and 21521091). C.S. acknowledges the supports from Guangdong Special Support Program and Shenzhen Peacock Plan (KQJSCX20170727100802505 and KQTD2016053112042971). J.T. acknowledges the support from Agency for Science, Technology and Research (A*STAR) under Grant No. 1527000014. We acknowledge the fruitful discussion with Prof. Dr. W. H. Eugen Schwarz. The calculations were performed by using the supercomputers at Tsinghua National Laboratory for Information Science and Technology and SUSTech supercomputer center. F.-C.C. acknowledges support from the National Center for Theoretical Sciences and the Ministry of Science and Technology of Taiwan under Grant No. MOST-107-2628-M-110-001-MY3. F.-C.C. is also grateful to the National Center for High-performance computing for computer time and facilities.

Conflict of interest

The authors declare no conflict of interest.

Stichwörter: Atomare Präzision · Emissionsverstärkung · Goldnanocluster · Oberflächengestaltung

[1] a) R. Jin, C. J. Zeng, M. Zhou, Y. X. Chen, *Chem. Rev.* **2016**, *116*, 10346; b) J. Z. Yan, B. K. Teo, N. F. Zheng, *Acc. Chem. Res.* **2018**, *51*, 3084; c) I. Chakraborty, T. Pradeep, *Chem. Rev.* **2017**, *117*, 8208; d) C. M. Aikens, *Acc. Chem. Res.* **2018**, *51*, 3065; e) S. Knoppe, T. Burgi, *Acc. Chem. Res.* **2014**, *47*, 1318; f) S. Hossain, Y. Niihori, L. V. Nair, B. Kumar, W. Kurashige, Y. Negishi, *Acc. Chem. Res.* **2018**, *51*, 3114; g) C. Y. Yi, M. A. Tofanelli, C. J. Ackerson, K. L. Knappenberger, *J. Am. Chem. Soc.* **2013**, *135*, 18222; h) Q. Tang, G. X. Hu, V. Fung, D. E. Jiang, *Acc. Chem. Res.* **2018**, *51*, 2793; i) R.-W. Huang, Y.-S. Wei, X.-Y. Dong, X.-H. Wu, C.-X. Du, S.-Q. Zang, T. C. W. Mak, *Nat. Chem.* **2017**, *9*, 689; j) R.-W. Huang, X.-Y. Dong, B.-J. Yan, X.-S. Du, D.-H. Wei, S.-Q. Zang, T. C. W. Mak, *Angew. Chem. Int. Ed.* **2018**, *57*, 8560; *Angew. Chem.* **2018**, *130*, 8696.

[2] a) Z. Wu, R. Jin, *Nano Lett.* **2010**, *10*, 2568; b) R. Itteboina, U. D. Madhuri, P. Ghosal, M. Kannan, T. K. Sau, T. Tsukuda, S. Bhardwaj, *J. Phys. Chem. A* **2018**, *122*, 1228; c) T. P. Bigioni, R. L. Whetten, Ö. Dag, *J. Phys. Chem. B* **2000**, *104*, 6983; d) G. Wang, T. Huang, R. W. Murray, L. Menard, R. G. Nuzzo, *J. Am. Chem. Soc.* **2005**, *127*, 812.

[3] a) G. Pramanik, J. Humpolickova, J. Valenta, P. Kundu, S. Bals, P. Bour, M. Dracinsky, P. Cigler, *Nanoscale* **2018**, *10*, 3792; b) S. Wang, X. Meng, A. Das, T. Li, Y. Song, T. Cao, X. Zhu, M. Zhu, R. Jin, *Angew. Chem. Int. Ed.* **2014**, *53*, 2376; *Angew. Chem.* **2014**, *126*, 2408; c) Z. Luo, X. Yuan, Y. Yu, Q. Zhang, D. T. Leong, J. Y. Lee, J. Xie, *J. Am. Chem. Soc.* **2012**, *134*, 16662; d) N. Goswami, Q. Yao, Z. Luo, J. Li, T. Chen, J. Xie, *J. Phys. Chem. Lett.* **2016**, *7*, 962; e) K. Pyo, V. D. Thanthirige, K. Kwak, P. Pandurangan, G. Ramakrishna, D. Lee, *J. Am. Chem. Soc.* **2015**, *137*, 8244; f) Z. Gan, Y. Lin, L. Luo, G. Han, W. Liu, Z. Liu, C. Yao, L. Weng, L. Liao, J. Chen, X. Liu, Y. Luo, C. Wang, S. Wei, Z. Wu, *Angew. Chem. Int. Ed.* **2016**, *55*, 11567; *Angew. Chem.* **2016**, *128*, 11739; g) T. Chen, S. Yang, J. Chai, Y. Song, J. Fan, B. Rao, H. Sheng, H. Yu, M. Zhu, *Sci. Adv.* **2017**, *3*, e1700956; h) M. Sugiuchi, J. Maeba, N. Okubo, M. Iwamura, K. Nozaki, K. Konishi, *J. Am. Chem. Soc.* **2017**, *139*, 17731; i) Z. Wang, H. F. Su, M. Kurmoo, C. H. Tung, D. Sun, L. S. Zheng, *Nat. Commun.* **2018**, *9*, 2094; j) X. Kang, S. Wang, Y. Song, S. Jin, G. Sun, H. Yu, M. Zhu, *Angew. Chem. Int. Ed.* **2016**, *55*, 3611; *Angew. Chem.* **2016**, *128*, 3675; k) M. S. Bootharaju, H. Chang, G. C. Deng, S. Malola, W. Baek, H. Hakkinen, N. F. Zheng, T. Hyeon, *J. Am. Chem. Soc.* **2019**, *141*, 8422; l) Z. P. Wang, Z. L. Zhu, C. K. Zhao, Q. F. Yao, X. Y. Li, H. Y. Liu, F. L. Du, X. Yuan, J. Xie, *Chem. Asian J.* **2019**, *14*, 765.

[4] a) M. Zhu, C. M. Aikens, F. J. Hollander, G. C. Schatz, R. Jin, *J. Am. Chem. Soc.* **2008**, *130*, 5883; b) M. W. Heaven, A. Dass, P. S. White, K. M. Holt, R. W. Murray, *J. Am. Chem. Soc.* **2008**, *130*, 3754; c) K. L. D. M. Weerawardene, C. M. Aikens, *J. Am. Chem. Soc.* **2016**, *138*, 11202; d) J. Akola, M. Walter, R. L. Whetten, H. Haekkinen, H. Groenbeck, *J. Am. Chem. Soc.* **2008**, *130*, 3756; e) P. N. Day, R. Pachter, K. A. Nguyen, R. Jin, *J. Phys. Chem. A* **2019**, *123*, 6472; f) Y. Shichibu, Y. Negishi, T. Tsukuda, T. Teranishi, *J. Am. Chem. Soc.* **2005**, *127*, 13464.

[5] a) M. Walter, J. Akola, O. Lopez-Acevedo, P. D. Jadzinsky, G. Calero, C. J. Ackerson, R. L. Whetten, H. Gronbeck, H. Hakkinen, *Proc. Natl. Acad. Sci. USA* **2008**, *105*, 9157; b) K. L. D. M. Weerawardene, P. Pandeya, M. Zhou, Y. Chen, R. Jin, C. M. Aikens, *J. Am. Chem. Soc.* **2019**, *141*, 18715.

[6] a) C. Yao, Y.-j. Lin, J. Yuan, L. Liao, M. Zhu, L.-h. Weng, J. Yang, Z. Wu, *J. Am. Chem. Soc.* **2015**, *137*, 15350; b) S. Wang, Y. Song, S. Jin, X. Liu, J. Zhang, Y. Pei, X. Meng, M. Chen, P. Li, M. Zhu, *J. Am. Chem. Soc.* **2015**, *137*, 4018; c) Q. Li, K. J. Lambright, M. G. Taylor, K. Kirschbaum, T.-Y. Luo, J. Zhao, G. Mpourmpakis, S. Mokashi-Punekar, N. L. Rosi, R. Jin, *J. Am. Chem. Soc.* **2017**, *139*, 17779; d) S. Yang, S. Chen, L. Xiong, C. Liu, H. Yu, S. Wang, N. L. Rosi, Y. Pei, M. Zhu, *J. Am. Chem. Soc.* **2018**, *140*, 10988; e) M. Zhu, P. Wang, N. Yan, X. Chai, L. He, Y. Zhao, N. Xia, C. Yao, J. Li, H. Deng, Y. Zhu, Y. Pei, Z. Wu, *Angew. Chem. Int. Ed.* **2018**, *57*, 4500; *Angew. Chem.* **2018**, *130*, 4590.

[7] a) R. S. Dhayal, J.-H. Liao, Y.-C. Liu, M.-H. Chiang, S. Kahlal, J.-Y. Saillard, C. W. Liu, *Angew. Chem. Int. Ed.* **2015**, *54*, 3702; *Angew. Chem.* **2015**, *127*, 3773; b) A. Desireddy, B. E. Conn, J. Guo, B. Yoon, R. N. Barnett, B. M. Monahan, K. Kirschbaum, W. P. Griffith, R. L. Whetten, U. Landman, T. P. Bigioni, *Nature* **2013**, *501*, 399; c) X.-K. Wan, W. W. Xu, S.-F. Yuan, Y. Gao, X.-C. Zeng, Q.-M. Wang, *Angew. Chem. Int. Ed.* **2015**, *54*, 9683; *Angew. Chem.* **2015**, *127*, 9819.

[8] a) D. Lee, R. L. Donkers, G. L. Wang, A. S. Harper, R. W. Murray, *J. Am. Chem. Soc.* **2004**, *126*, 6193; b) L. Liao, S. Zhou, Y. Dai, L. Liu, C. Yao, C. Fu, J. Yang, Z. Wu, *J. Am. Chem. Soc.* **2015**, *137*, 9511.

[9] C. Yao, S. Tian, L. Liao, X. Liu, N. Xia, N. Yan, Z. Gan, Z. Wu, *Nanoscale* **2015**, *7*, 16200.

[10] a) Y. Q. Dong, J. W. Y. Lam, A. J. Qin, Z. Li, J. Z. Sun, H. H. Y. Sung, I. D. Williams, B. Z. Tang, *Chem. Commun.* **2007**, 40; b) X. L. Luo, J. N. Li, C. H. Li, L. P. Heng, Y. Q. Dong, Z. P. Liu, Z. S. Bo, B. Z. Tang, *Adv. Mater.* **2011**, *23*, 3261.

[11] a) E. S. Shibu, M. A. H. Muhammed, T. Tsukuda, T. Pradeep, *J. Phys. Chem. C* **2008**, *112*, 12168; b) T. D. Green, C. Yi, C. Zeng, R. Jin, S. McGill, K. L. Knappenberger, Jr., *J. Phys. Chem. A* **2014**, *118*, 10611.

[12] a) C. M. Aikens, *J. Phys. Chem. C* **2008**, *112*, 19797; b) S. F. Yuan, C. Q. Xu, J. Li, Q. M. Wang, *Angew. Chem. Int. Ed.* **2019**, *58*, 5906; *Angew. Chem.* **2019**, *131*, 5967; c) F. K. Sheong, J.-X. Zhang, Z. Lin, *Inorg. Chem.* **2016**, *55*, 11348.

[13] M. Ebina, T. Iwasa, Y. Harabuchi, T. Taketsugu, *J. Phys. Chem. C* **2018**, *122*, 4097.

[14] C.-Y. Liu, H.-F. Wang, Z.-G. Ren, P. Braunstein, J.-P. Lang, *Inorg. Chem.* **2019**, *58*, 8533.

[15] K. L. D. M. Weerawardene, E. B. Guidez, C. M. Aikens, *J. Phys. Chem. C* **2017**, *121*, 15416.

Manuskript erhalten: 20. Januar 2020
Akzeptierte Fassung online: 30. Januar 2020
Endgültige Fassung online: ■■. ■■ ■■■■

Forschungsartikel

Nanocluster

C. Yao, C.-Q. Xu, I.-H. Park, M. Zhao, Z. Zhu, J. Li, X. Hai, H. Fang, Y. Zhang, G. Macam, J. Teng, L. Li, Q.-H. Xu, F.-C. Chuang, J. P. Lu, C. Su,* J. Li,* J. Lu* ——— ■■■■–■■■■

Giant Emission Enhancement of Solid-State Gold Nanoclusters by Surface Engineering

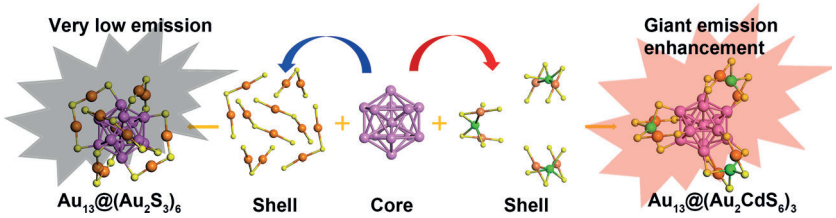

Mehr Schein: Eine ligandeninduzierte Umgestaltung der Oberfläche durch Dotierung mit Heteroatomen wurde genutzt, um die Oberfläche eines prototypischen $[Au_{25}(SR^1)_{18}]^-$-Clusters präzise zu modifizieren und dabei dessen ikosaedrischen Au_{13}-Kern zu bewahren. Dies führte zu dem neuen Dimetallcluster $[Au_{19}Cd_3(SR^2)_{18}]^-$.